ACS OMEGA

Article

Cite This: ACS Omega 2019, 4, 15043−15050

http://pubs.acs.org/journal/acsodf

Double-Crosslinked GO Interlayer Framework as a Pervaporation Hybrid Membrane with High Performance

Xin Zhang,[†] Ming-Xiao Zhang,[†] Hao Ding,[†] Hu Yang,[†] Xiao-Hua Ma,*[,†] Xin-Ru Xu,[†] Zhen-Liang Xu,[†] and Chuyang Y. Tang[‡,§,∥]

[†]Shanghai Key Laboratory of Multiphase Materials Chemical Engineering, Membrane Science and Engineering R&D Lab, Chemical Engineering Research Center, School of Chemical Engineering, East China University of Science and Technology, 130 Meilong Road, Shanghai 200237, China

[‡]UNESCO Centre for Membrane Science and Technology, School of Chemical Engineering and [§]UNSW Water Research Centre, School of Civil and Environmental Engineering, University of New South Wales, Sydney, New South Wales 2052, Australia

[∥]Department of Civil Engineering, The University of Hong Kong, Pokfulam Road, Hong Kong S.A.R. 999077, China

Supporting Information

ABSTRACT: Graphene oxide (GO), as a two-dimensional structure material, has attracted widespread attention in the field of molecule sieving. However, GO-based membranes usually exhibit undesirable separation performance because the microstructure of GO is difficult to adjust. Herein, a novel double-crosslinking strategy for tuning the interlayer spacing of GO is reported. The hybrid membrane fabricated by the double-crosslinking strategy was used for pervaporation (PV) dehydration of isopropanol. To achieve high-performance of the PV hybrid membranes, the effects of operating cycles, chitosan concentration, and GO concentration were systematically investigated. The PV hybrid membranes were characterized by Fourier transform infrared spectroscopy, X-ray photoelectron spectroscopy, water contact angle measurement, and scanning electron microscopy. The results demonstrate that the interlayer of GO can be adjusted successfully by the double-crosslinking strategy. The fabricated hybrid membrane containing 0.1 wt % GO exhibited excellent performance with a flux of 4391 g/m^{2}h and a separation factor of 1491, which indicated that the double-crosslinking strategy may extend the applications of GO in the field of membrane separation.

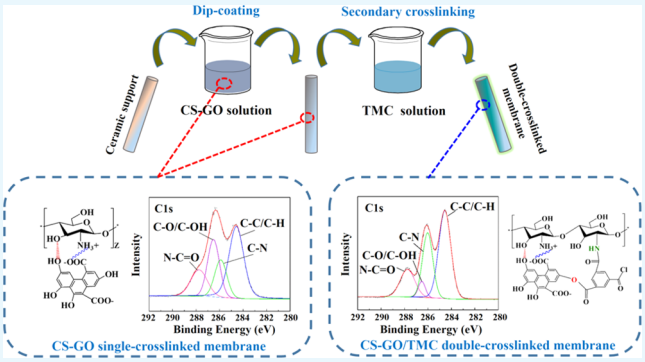

1. INTRODUCTION

Pervaporation possesses great potential to separate liquids, especially for azeotropic and close boiling point mixtures. Isopropanol (IPA), as a basic chemical raw material and solvent, is widely applied in the pharmaceutical and chemical industries.[1,2] To obtain high-purity IPA, many traditional technologies such as extractive distillation, molecular sieve absorption, and azeotrope distillation as well as pervaparation have been studied.[3] Among them, pervaporation gets a great deal of attention due to its advantages of easy operation, energy saving, high efficiency, and environment friendly.[4−7] The critical link for the full utilization of pervaporation is the development of pervaporation membranes.[8,9]

Graphene oxide (GO) is a two-dimensional material derived from graphite. Owing to its defined channel dimensions, excellent transport capabilities and outstanding molecular sieving properties,[10,11] GO has shown great potential for water desalination,[12,13] electrochemical energy storage,[14,15] gas separation,[16] and bioseparation[17] and biofouling control.[18]

To further extend its application in the field of membranes, great efforts have been focused on tuning the interlayer spacing of GO by physical approaches (e.g., intercalating with other nanomaterials[19] and introducing membrane porosity[20,21]) and chemical strategies (adding cations in the membrane matrix[22,23]). For instance, improved water permeation was achieved for composite GO-framework membranes by the incorporation of GO in the poly(vinyl alcohol) solution.[24] Templating the GO framework with copper hydroxide nanostrands and their subsequent removal by ethylenediaminetetraacetic acid resulted in an enhanced porous structure that led to a 10-fold enhancement in flux.[25] For chemical modification of GO, researchers often take advantages of the abundant active oxygen-containing functional groups[26−28] on GO to adjust the interlayer spacing. Chen et al.[11] demonstrated that intercalation of cations in GO can effectively control the interlayer spacing and thus efficiently improve the performance of GO membranes. Based on these

Received: June 20, 2019
Accepted: August 23, 2019
Published: September 6, 2019

DOI: 10.1021/acsomega.9b01833
ACS Omega 2019, 4, 15043−15050

recent achievements, the application of GO materials possesses great potential in the membrane field.[29]

In this study, a novel double-crosslinking strategy was reported for tuning the interlayer spacing of GO to further improve the pervaporation performance of a GO-based membrane. First, chitosan (CS) was used as a binder of GO nanosheets owing to the presence of hydrogen bonds and electrostatic interactions between them. Then, a secondary crosslinking between CS and GO was conducted using trimesoyl chloride (TMC) as a crosslinking agent. The GO membranes fabricated by the double-crosslinking strategy were characterized by Fourier transform infrared (FTIR) spectroscopy and X-ray photoelectron spectroscopy (XPS) analyses; besides, its physiochemical properties were compared with its single-crosslinked counterpart. The results of FTIR and XPS indicated the increase of hydrogen bonds and presence of electrostatic interactions in the membrane matrix. The fabricated hybrid membranes exhibited excellent separation performance (pervaporation separation index (PSI) value of 8.5×10^6) for isopropanol (IPA) dehydration, which underpinned its great potential for the novel double-crosslinking approach.

2. RESULTS AND DISCUSSION

2.1. Characterization of GO-Based Crosslinking Membranes. To investigate the chemical properties (e.g., crosslinking) of GO membranes, different membranes including the pure CS membrane, CS−GO single-crosslinked membrane, and CS−GO/TMC double-crosslinked membrane were fabricated on Al_2O_3 ceramic supports and characterized by FTIR as in Figure 1. The FTIR absorption peaks of several

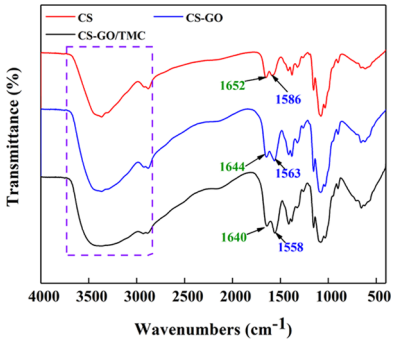

Figure 1. FTIR spectra of CS, CS−GO, and CS−GO/TMC membranes. The CS, GO, and TMC concentrations of the crosslinking membranes were 1.0, 0.1, and 0.5 wt %, respectively.

major groups are summarized in Table S1.[30] Compared with pure CS membranes, the peak positions of the CS−GO single-crosslinked membranes present red shift phenomena. Furthermore, the peak positions of C═O and N−H groups of double-crosslinked CS−GO/TMC membranes present a more obvious red shift phenomenon (Figure 1). Moreover, the area ratios of C═O and N−H groups on crosslinked membranes are less than 1 (Table S1). These observations can be explained by the electrostatic interaction between the carboxyl (−COOH) on the GO and the amidogen ($-NH_2$) on the CS (see Figure 3a),[31] successfully crosslinking between the acyl chloride groups (O═C−Cl) and $-NH_2$ on the CS[32,33] (Figure S1). In addition, the absorption band of −OH broadens, indicating an increase of the number of hydrogen bonds in the membrane matrix.[34,35]

Figure 2 and Table 1 present the chemical compositions[36,37] and chemical bond content of various membranes, respectively, through XPS analysis. High-resolution XPS analysis of the C 1s peak shows that the peak area percentage of the N−C═O bond decreases from 17.1% for CS to 15.8% for CS−GO. Similarly, that of the C−N bond reduces from 20.7 to 16.7%. This result could be partially explained by the interaction between the amidogen ($-NH_2$) on the CS with the carboxyl (−COOH) on the GO (see Figure 3a) in addition to the dilution effect by blending CS with GO. Furthermore, the content of C−O/C−OH bonds increases from 18.8 to 24.9% and the carbon atom content increases from 35.8 to 54.9% because of the successful incorporation of GO in the CS solution. The XPS wide-scan in Figure 2b shows 4.0% of the Al 2p signal that originated from the Al_2O_3 ceramic support. This indicates that the CS−GO membrane has significant defects.

The XPS spectra of the CS−GO/TMC membranes are shown in Figure 2c. The content of C−O/C−OH bonds dramatically reduces from 24.9 to 5.0% (Table 1), which is consistent with the chemical crosslinking of CS−GO by TMC (e.g., the reaction between hydroxyls (−OH) on CS−GO and acryl chloride groups (O═C−Cl) on TMC as shown in Figure 3b). In addition, the Al 2p signal can no longer be detected for the CS−GO/TMC membrane, indicating the formation of an intact separation layer on the ceramic support.

Based on the results of XPS analysis, the CS−GO single-crosslinking membrane has some drawbacks due to the existence of the Al 2p signal. Therefore, the water contact angles of the double-crosslinking membranes were measured to highlight the effect of GO on membrane hydrophilicity as compared with that of the CS/TMC single-crosslinking membrane. The water contact angles of CS−GO^Y/TMC membranes are illustrated in Figure 4, where Y represents GO concentration. The water contact angle at any given time followed the order of: CS−$GO^{0.2}$/TMC< CS−$GO^{0.1}$/TMC < CS−$GO^{0.3}$/TMC < CS/TMC. This demonstrates that GO plays a dual role in the hydrophilicity of the hybrid membranes. The water contact angle decreases with increased GO concentration when GO concentration is less than 0.2 wt % on account of the water channels provided by GO containing many hydrophilic functional groups. However, the contact angle increases when GO concentration is greater than 0.2 wt %, which is detrimental to the hydrophilicity of hybrid membranes. A possible reason for this phenomenon is that enhanced interactions[24] between CS molecules and GO sheets hamper the permeation of water.

The effect of GO concentration (Y) on the cross-section and outside surface morphologies of the CS−GO^Y/TMC hybrid membranes is demonstrated in Figure 5. The particle-like texture of the Al_2O_3 substrate is clearly presented in the scanning electron microscopy (SEM) images when no or 0.1 wt % GO concentration was used (Figure 5b,d), which was consistent with the formation of relatively thin rejection layers under these conditions (Figure 5a,c). As the GO concentration increases, the texture of the substrate disappears gradually (Figure 5f,h) and the laminate membrane structure of GO is clearly visible (Figure 5e,g). However, the rejection layers became thicker.

The effect of CS concentration (X) on the morphologies of the CS^X−GO/TMC hybrid membranes is shown in Figure 6. The thickness of the rejection layer increases with the increase of CS concentration, which is similar to the effect of increasing GO concentration (Figure 5). At a CS concentration of 3.0 wt

DOI: 10.1021/acsomega.9b01833
ACS Omega 2019, 4, 15043−15050

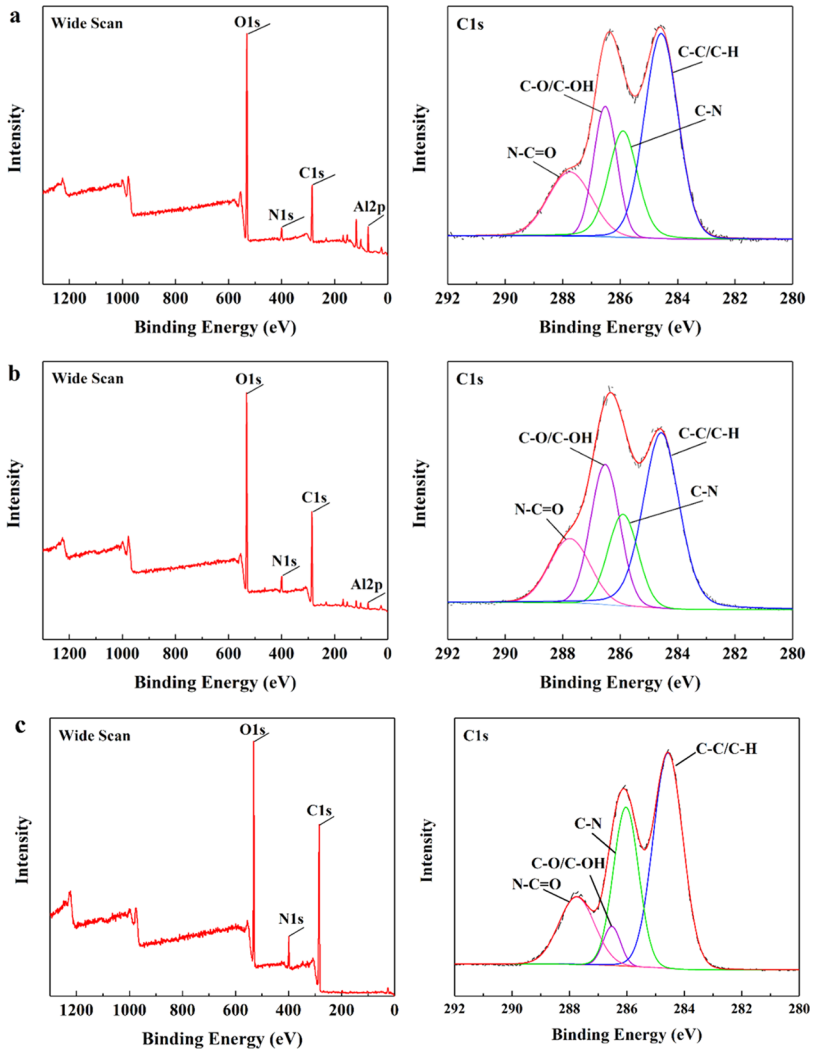

Figure 2. XPS wide-scan and C 1s core level of (a) CS, (b) CS−GO, and (c) CS−GO/TMC membranes. The CS, GO, and TMC concentrations of the hybrid membranes were 1.0, 0.1, and 0.5 wt %, respectively.

Table 1. Elemental and Chemical Bond Composition of Pure CS, CS−GO, and CS−GO/TMC Membranes Analyzed by XPS[a]

	atoms percent (%)				chemical bond percent (%)			
item	C 1s	N 1s	O 1s	Al 2p	N−C═O	C−O/C−OH	C−N	C−C/C-H
binding energy (eV)	285.2	399.4	532.5	74.1	287.7	286.5	285.9	284.6
CS	35.8	4.5	43.3	16.3	17.1	18.8	20.7	43.4
CS−GO	54.9	5.8	35.3	4.0	15.8	24.9	16.7	42.6
CS−GO/TMC	66.1	6.0	27.9		17.6	5.0	29.4	48.0

[a]The CS and TMC concentrations of the hybrid membranes were 1.0 and 0.5 wt %, respectively

%, the membrane surface appears to be smooth (Figure 6h), which can be explained by the increased viscosity of the CS−GO mixture at higher CS concentrations (see Figure S2).

The morphologies of the cross-section and surface of CS−GO/TMC/N membranes are shown in Figure 7, where N represents the number of operating cycles of the double-crosslinking membrane prepared on ceramic support. At a low number of operating cycles (e.g., 1), there are obvious defects on the surface of the CS−GO/TMC/1 hybrid membrane: the rough surface of the ceramic support cannot even be entirely covered (Figure 7a,b). Increasing the number of operating cycles (e.g., 2−4) results in the formation of an intact rejection layer (Figure 7c−h). In addition, no apparent delamination between the rejection layer and the support can be observed owing to the presence of hydrogen bonds between the surface active layer and ceramic support.

2.2. Pervaporation Dehydration Performance of Hybrid Membranes. The pure CS and single-crosslinked CS−GO membranes did not exhibit a separation effect for the water−IPA mixture when the concentration of CS is low. Therefore, the double-crosslinked GO-framework membranes were used to separate the water−IPA mixtures via PV at 60 °C. Various factors for the separation performance of the membranes were investigated, such as the GO concentration, CS concentration, and number of operation cycles.

DOI: 10.1021/acsomega.9b01833
ACS Omega 2019, 4, 15043−15050

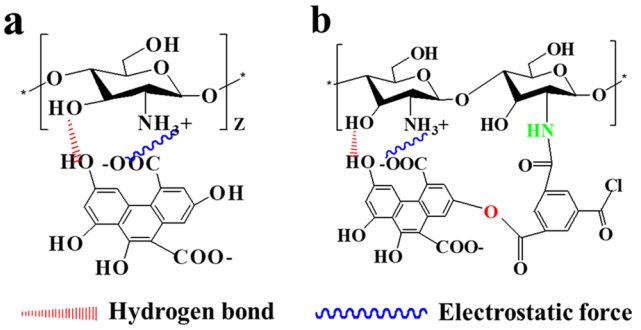

Figure 3. (a) Single-crosslinking mechanism of CS−GO and (b) double-crosslinking mechanism of CS−GO/TMC.

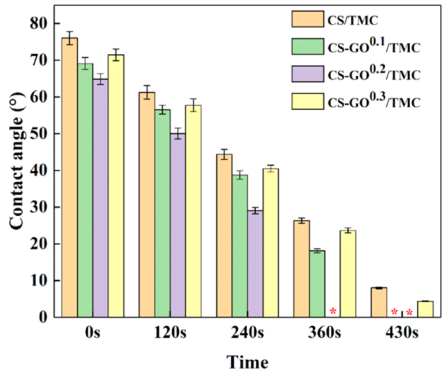

Figure 4. Water contact angles of CS/TMC, CS−$GO^{0.1}$/TMC, CS−$GO^{0.2}$/TMC, and CS−$GO^{0.3}$/TMC membranes. The symbol (*) in the figure indicates perfect wetting (contact angle ≈ 0°). The CS and TMC concentrations were 1.0 and 0.5 wt %, respectively.

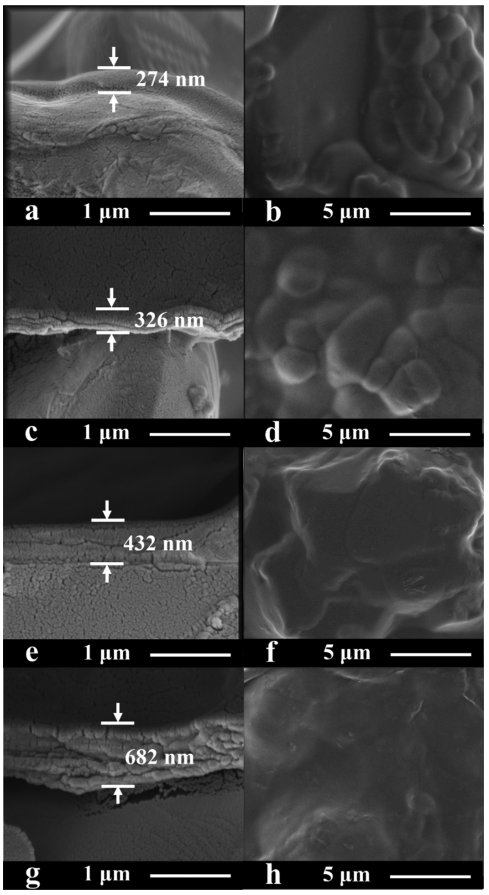

Figure 5. Cross-sectional and surface SEM images of (a, b) CS/TMC, (c, d) CS−$GO^{0.1}$/TMC, (e, f) CS−$GO^{0.2}$/TMC, and (g, h) CS−$GO^{0.3}$/TMC membranes. The CS and TMC concentrations were 1.0 and 0.5 wt %, respectively. The number of operating cycles was 3.

The PV performance of the hybrid membranes with different GO concentrations is shown in Figure 8. The separation factor increases when the GO concentration increases from 0 to 0.3 wt %, while the flux first increases and then decreases. A possible explanation is that GO plays a dominant role in providing passages for water penetration at first. However, the function of GO is weakened and the transmembrane resistance plays a great role with the increase of membrane thickness (Figure 5). Besides the increased membrane thickness, another main reason for increased separation factor is the formation of a more laminate structure (Figure 5g) of GO with increased GO concentration. Such a laminate structure is preferred for the transport of water molecules.[38]

From Figure 9, the flux of the hybrid membranes decreases gradually while the separation factor increases with the increase of CS concentration, which demonstrates that CS concentration plays an important role in the pervaporation performance of the hybrid membranes. The higher the CS concentration is, the thicker the membrane becomes, resulting in the increase of transmembrane resistance of the hybrid membranes.[28] However, increased membrane thickness is of benefit to form an intact separation layer, leading to an increased separation factor.

The effect of the operating cycles on the PV performance of the hybrid membranes is shown in Figure 10. The flux is 18.0 kg/m^2h with a separation factor of merely 5.5 when the number of operating cycles is only once, which echoes the presence of some surface defects on the hybrid membrane (Figure 7b). With the increase of the number of operating cycles, the membrane flux decreases slightly while the separation factor increases significantly. An intact separation layer is required to ensure the excellent separation performance of the hybrid membranes for IPA−water separation. As the membrane thickness increased, an intact separation layer was generated on the surface, guaranteeing the gradual increase of the separation factor, the effect of which was similar to that of the increase in CS concentration.

The long-term stability of the GO-based membrane was investigated by separating 90 wt % IPA aqueous solution at 60 °C. From Figure 11, both the membrane flux and separation factor remain nearly unchanged during the operation for 100 h, which illustrates that the hybrid membranes fabricated by the double-crosslinking strategy exhibit good durability.

2.3. PV Performance Comparison. The PV performances of the hybrid membranes in this work are compared with those in the literature (Table 2). It is obvious that the double-crosslinking membranes in this study exhibit excellent separation performances and great potential in IPA dehydration.

3. CONCLUSIONS

A series of GO-framework membranes were successfully fabricated by the double-crosslinking strategy for PV dehydration of IPA. FTIR, XPS, SEM, water contact angle and PV tests were used to investigate the physicochemical properties, morphologies, hydrophilicity, and separation

DOI: 10.1021/acsomega.9b01833
ACS Omega 2019, 4, 15043−15050

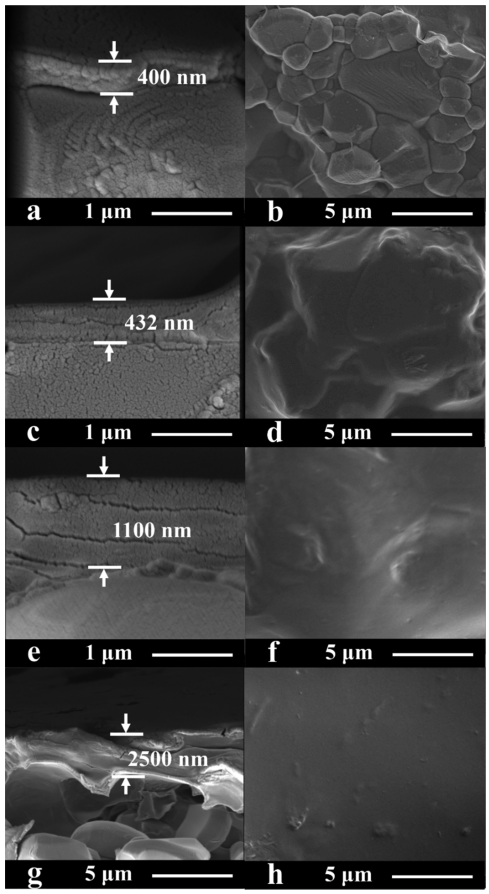

Figure 6. Cross-sectional and surface SEM images of (a, b) $CS^{0.5}$–GO/TMC, (c, d) $CS^{1.0}$–GO/TMC, (e, f) $CS^{2.0}$–GO/TMC, and (g, h) $CS^{3.0}$–GO/TMC membranes. The GO and TMC concentrations were 0.2 and 0.5 wt %, respectively. The number of operating cycles was 3.

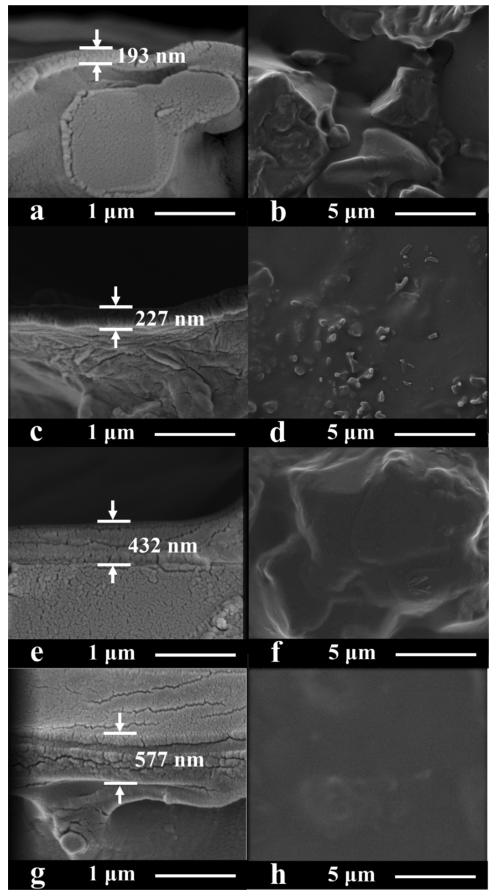

Figure 7. Cross-sectional and surface SEM images of (a, b) CS–GO/TMC/1, (c, d) CS–GO/TMC/2, (e, f) CS–GO/TMC/3, and (g, h) CS–GO/TMC/4 membranes. The CS, GO, and TMC concentrations were 1.0, 0.2, and 0.5 wt %, respectively.

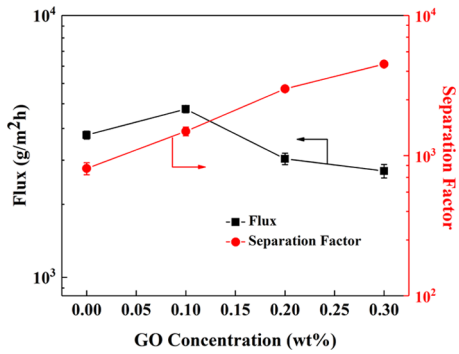

Figure 8. PV performance of CS/TMC, CS–$GO^{0.1}$/TMC, CS–$GO^{0.2}$/TMC, and CS–$GO^{0.3}$/TMC hybrid membranes. The CS and TMC concentrations in the hybrid membranes were 1.0 and 0.5 wt %, respectively. The number of operating cycles was 3.

performance of the obtained membranes. The FTIR and XPS results reveal the formation of hydrogen bonds between GO and CS and the successful crosslinking between CS–GO and TMC. The GO in the membrane matrix provides selective water passages, which results in an excellent membrane flux. The successful crosslinking between CS–GO and TMC ensures excellent separation performance for IPA dehydration. Therefore, the fabricated hybrid membranes provide a useful reference to develop novel PV membranes and great potential for the dehydration of alcohol.

4. EXPERIMENTAL SECTION

4.1. Materials. Chitosan (CS, 50–100 mPa at 20 °C, the deacetylation degree > 80%) was obtained from Titan Scientific Co., Ltd. Shanghai, China. Acetic acid (HAc, AR, ≥99.5 wt %) and isopropanol (IPA, AR, ≥99.7 wt %) were purchased from Sinopharm Chemical Reagent Co., Ltd. Shanghai, China. Trimesoyl chloride (TMC, ≥99.8 wt %) was received from Qingdao Benzo Chemical Company, China. Ceramic supporting membranes with a mean pore diameter of 0.9 μm,[45] graphene oxide,[46] and deionized water were prepared in our laboratory.

4.2. Fabrication of the CS–GO Crosslinking Solution. First, 0.5–3.0 wt % CS solutions were prepared by dissolving certain mass of CS in 2.0 wt % HAc solution at room temperature. After the CS was completely dissolved, the prepared GO solution was added into the CS solution three times. During this process, the CS–GO mixed solution was stirred and treated by ultrasound to ensure the fabrication of the single-crosslinked GO framework.

4.3. Fabrication of CS–GO/TMC Hybrid Membranes. The ceramic hollow fiber membrane was selected as a support because of its high selectivity, permeability, thermal stability, and mechanical stability.[47,48] A membrane testing module was fabricated first, and the preparation procedures could be obtained from previous papers.[49,50] The fabricated membrane

DOI: 10.1021/acsomega.9b01833
ACS Omega 2019, 4, 15043–15050

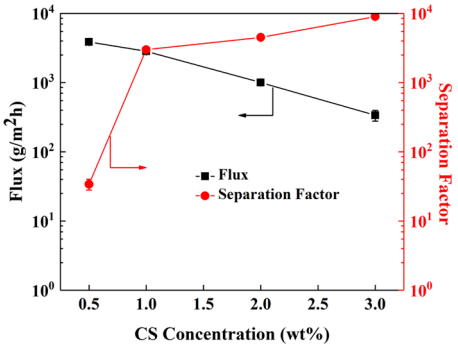

Figure 9. PV performance of $CS^{0.5}$–GO/TMC, $CS^{1.0}$–GO/TMC, $CS^{2.0}$–GO/TMC, and $CS^{3.0}$–GO/TMC hybrid membranes. The GO and TMC concentrations in the hybrid membranes were 0.2 and 0.5 wt %, respectively. The number of operating cycles was 3.

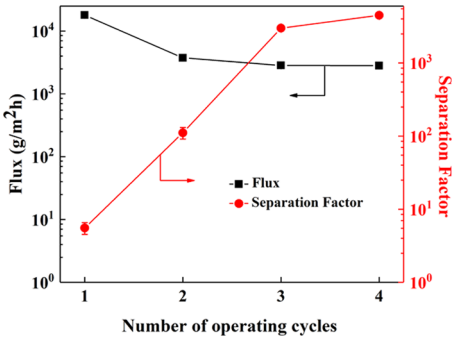

Figure 10. PV performance of CS–GO/TMC/1, CS–GO/TMC/2, CS–GO/TMC/3, and CS–GO/TMC/4 hybrid membranes. The CS, GO, and TMC concentrations in the hybrid membranes were 1.0, 0.2, and 0.5 wt %, respectively.

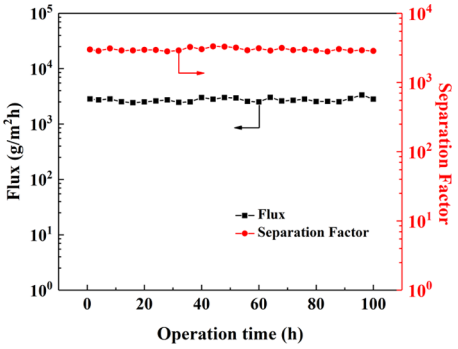

Figure 11. Long-term operation stability of $CS^{1.0}$–$GO^{0.2}$/TMC/3 hybrid membranes for separating 90 wt % IPA aqueous solution at 60 °C.

testing modules were immersed in the CS–GO crosslinking solution for 4 min. The excess CS–GO solution on the outside surface of the ceramic support was blown away by a circular air knife which ensured the uniformity and unity of the mixed solution on the ceramic support. Then, the membrane testing modules were immersed in TMC organic solution for 4 min, and the second crosslinking reaction between CS–GO and TMC occurred during the immersion time. The fabricated hybrid membranes were placed in a 75 °C oven for 5 min to allow further reaction. The above process was remarked as a cycle and repeated several times for formation of dense nondefective membranes, which was shown in Figure 12. The prepared membranes are denoted CS^X–GO^Y/TMC/N, where superscripts *X* and *Y* mean the mass concentration of CS and GO, respectively, and N means the number of operating cycles.

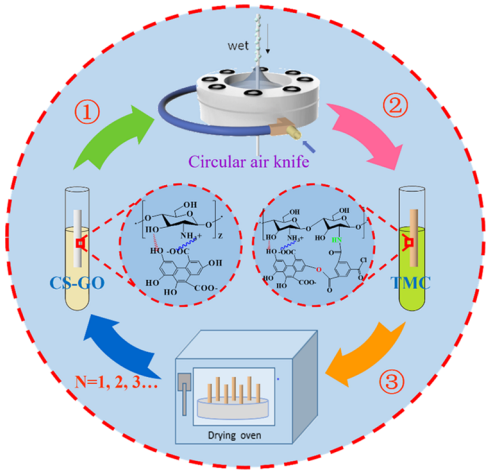

Figure 12. Schematic illustration of the preparation process of the CS–GO/TMC hybrid membrane.

4.4. Characterization. The surface chemical compositions of the crosslinking membranes were analyzed by Fourier transform infrared (FTIR, Nicolet-6700) spectroscopy and X-ray photoelectron spectroscopy (XPS, VG-Miclab II, U.K.). The hydrophilicity of hybrid membranes was determined by a contact angle meter (JC2000A, Shanghai Zhong Cheng Digital Equipment Co., Ltd, China) at room temperature. Membrane morphologies containing cross-sections with a magnification of 50 000 and surfaces with a magnification of 10 000 were observed by field-emission scanning electron microscopy (SEM, Nova NanoSEM 450).

4.5. PV Experiments. The PV performance of the hybrid membranes was investigated in dehydrating a 90 wt % IPA–H_2O mixture at 60 °C. The PV experiment was conducted by a

Table 2. PV Performance Comparison with the Existing PV Hybrid Membranes in the Literature

item	mass % of IPA in feed	operation temperature (°C)	flux (g/m²h)	separation factor	PSI (g/m²h)	reference
$CS^{1.0}$–$GO^{0.1}$/TMC/3	90	60	4391	1491	6.5×10^6	this work
$CS^{1.0}$–$GO^{0.2}$/ TMC/3	90	60	2835	2991	8.5×10^6	this work
CS/PTFE	70	70	1730	775	1.3×10^6	39
GO/mPAN	70	70	4137	1164	4.8×10^6	40
GO/mPAN	70	30	2047	2331	4.8×10^6	40
SA/CS wrapped MWCNTs	90	30	218	6420	1.4×10^6	41
CS/TGDMP	90	30	73.7	1050	7.7×10^4	42
SiO_2/PEC	90	70	2100	2186	4.6×10^6	43
Nexar block copolymer/Ultem	85	50	2440	221	5.4×10^5	44

DOI: 10.1021/acsomega.9b01833
ACS Omega 2019, 4, 15043–15050

self-made apparatus.[49,51] The permeate side of the hybrid membranes was maintained at a pressure of −0.1 MPa throughout the experiment. The composition of the permeate solution was analyzed by gas chromatography (Techcomp GC7890T, China). The membrane flux (J), separation factor (α), and pervaporation separation index (PSI) were calculated by the following formulas.[52]

$$J = W/(A \times t) \quad (1)$$

$$\alpha = (Y_w/Y_e)/(X_w/X_e) \quad (2)$$

$$\mathrm{PSI} = J \times (\alpha - 1) \quad (3)$$

where W is the total weight of permeate vapor (g), A is the effective membrane area (m^2), and t is the permeation time (h), Y_w/Y_e is the mass percentages of water to ethanol in permeate, and X_w/X_e is that in feed.

■ ASSOCIATED CONTENT

Supporting Information

The Supporting Information is available free of charge on the ACS Publications website at DOI: 10.1021/acsomega.9b01833.

Location and area ratio of absorption peaks in FTIR spectra (Table S1); the crosslinking schematic of (a) CS, (b) CS−GO, (c) CS/TMC, and (d) CS−GO/TMC crosslinking membranes (Figure S1); the viscosity of CS with different concentrations (1.0−4.0 wt %) (Figure S2) (PDF)

■ AUTHOR INFORMATION

Corresponding Author

*E-mail: xiaohuama@ecust.edu.cn. Tel.: +86 21 64253670. Fax: +86 21 64252989.

ORCID

Hu Yang: 0000-0001-9411-2553

Xiao-Hua Ma: 0000-0002-3902-1808

Zhen-Liang Xu: 0000-0002-1436-4927

Chuyang Y. Tang: 0000-0002-7932-6462

Notes

The authors declare no competing financial interest.

■ ACKNOWLEDGMENTS

The authors gratefully acknowledge the research funding provided by the Hong Kong Scholars Program (No. XJ2015015), National Natural Science Foundation of China (21406060), Fundamental Research Funds for the Central Universities (WA1514305), and China Postdoctoral Science Foundation (2016M601527).

■ REFERENCES

(1) Boli, E.; Dimou, E.; Voutsas, E. Separation of the isopropanol-water azeotropic mixture using ionic liquids. *Fluid Phase Equilib.* **2018**, *456*, 77−83.

(2) Pulyalina, A.; Polotskaya, G.; Goikhman, M.; Podeshvo, I.; Chernitsa, B.; Kocherbitov, V.; Toikka, A. Novel approach to determination of sorption in pervaporation process: a case study of isopropanol dehydration by polyamidoimideurea membranes. *Sci. Rep.* **2017**, *7*, No. 8415.

(3) Kubaczka, A.; Kaminski, W.; Marszalek, J. Predicting mass fluxes in the pervaporation process using Maxwell-Stefan diffusion coefficients. *J. Membr. Sci.* **2018**, *546*, 111−119.

(4) Salehian, P.; Chung, T. S. Thermally treated ammonia functionalized graphene oxide/polyimide membranes for pervaporation dehydration of isopropanol. *J. Membr. Sci.* **2017**, *528*, 231−242.

(5) Liao, Y. L.; Hu, C. C.; Lai, J. Y.; Liu, Y. L. Crosslinked polybenzoxazine based membrane exhibiting in-situ self promoted separation performance for pervaporation dehydration on isopropanol aqueous solutions. *J. Membr. Sci.* **2017**, *531*, 10−15.

(6) Ma, X. H.; Xu, Z. L.; Liu, Y.; Sun, D. Preparation and characterization of PFSA-PVA-SiO2/PVA/PAN difunctional hollow fiber composite membranes. *J. Membr. Sci.* **2010**, *360*, 315−322.

(7) Ma, X. H.; Xu, Z. L.; Ji, C. Q.; Wei, Y. M.; Yang, H. Characterization, Separation Performance, and Model Analysis of STPP-Chitosan/PAN Polyelectrolyte Complex Membranes. *J. Appl. Polym. Sci.* **2011**, *120*, 1017−1024.

(8) Dharupaneedi, S. P.; Nataraj, S. K.; Nadagouda, M.; Reddy, K. R.; Shukla, S. S.; Aminabhavi, T. M. Membrane-based separation of potential emerging pollutants. *Sep. Purif. Technol.* **2019**, *210*, 850−866.

(9) Kamali, M.; Suhas, D. P.; Costa, M. E.; Capela, I.; Aminabhavi, T. M. Sustainability considerations in membrane-based technologies for industrial effluents treatment. *Chem. Eng. J.* **2019**, *368*, 474−494.

(10) Zhou, K. G.; Vasu, K. S.; Cherian, C. T.; Neek-Amal, M.; Zhang, J. C.; Ghorbanfekr-Kalashami, H.; Huang, K.; Marshall, O. P.; Kravets, V. G.; Abraham, J.; Su, Y.; Grigorenko, A. N.; Pratt, A.; Geim, A. K.; Peeters, F. M.; Novoselov, K. S.; Nair, R. R. Electrically controlled water permeation through graphene oxide membranes. *Nature* **2018**, *559*, 236−240.

(11) Chen, L.; Shi, G. S.; Shen, J.; Peng, B. Q.; Zhang, B. W.; Wang, Y. Z.; Bian, F. G.; Wang, J. J.; Li, D. Y.; Qian, Z.; Xu, G.; Liu, G. P.; Zeng, J. R.; Zhang, L. J.; Yang, Y. Z.; Zhou, G. Q.; Wu, M. H.; Jin, W. Q.; Li, J. Y.; Fang, H. P. Ion sieving in graphene oxide membranes via cationic control of interlayer spacing. *Nature* **2017**, *550*, 415−418.

(12) Sun, P. Z.; Zheng, F.; Zhu, M.; Song, Z. G.; Wang, K. L.; Zhong, M. L.; Wu, D. H.; Little, R. B.; Xu, Z. P.; Zhu, H. W. Selective Trans-Membrane Transport of Alkali and Alkaline Earth Cations through Graphene Oxide Membranes Based on Cation-pi Interactions. *ACS Nano* **2014**, *8*, 850−859.

(13) Lin, L. C.; Grossman, J. C. Atomistic understandings of reduced graphene oxide as an ultrathin-film nanoporous membrane for separations. *Nat. Commun.* **2015**, *6*, No. 8335.

(14) El-Kady, M. F.; Strong, V.; Dubin, S.; Kaner, R. B. Laser Scribing of High-Performance and Flexible Graphene-Based Electrochemical Capacitors. *Science* **2012**, *335*, 1326−1330.

(15) Raccichini, R.; Varzi, A.; Passerini, S.; Scrosati, B. The role of graphene for electrochemical energy storage. *Nat. Mater.* **2015**, *14*, 271−279.

(16) Jiang, D. E.; Cooper, V. R.; Dai, S. Porous Graphene as the Ultimate Membrane for Gas Separation. *Nano Lett.* **2009**, *9*, 4019−4024.

(17) Garaj, S.; Hubbard, W.; Reina, A.; Kong, J.; Branton, D.; Golovchenko, J. A. Graphene as a subnanometre trans-electrode membrane. *Nature* **2010**, *467*, No. 190.

(18) Zhu, J. Y.; Wang, J.; Hou, J. W.; Zhang, Y. T.; Liu, J. D.; Van der Bruggen, B. Graphene-based antimicrobial polymeric membranes: a review. *J. Mater. Chem. A* **2017**, *5*, 6776−6793.

(19) Goh, K.; Jiang, W. C.; Karahan, H. E.; Zhai, S. L.; Wei, L.; Yu, D. S.; Fane, A. G.; Wang, R.; Chen, Y. All-Carbon Nanoarchitectures as High-Performance Separation Membranes with Superior Stability. *Adv. Funct. Mater.* **2015**, *25*, 7348−7359.

(20) Sun, H. T.; Mei, L.; Liang, J. F.; Zhao, Z. P.; Lee, C.; Fei, H. L.; Ding, M. N.; Lau, J.; Li, M. F.; Wang, C.; Xu, X.; Hao, G. L.; Papandrea, B.; Shakir, I.; Dunn, B.; Huang, Y.; Duan, X. F. Three-dimensional holey-graphene/niobia composite architectures for ultrahigh-rate energy storage. *Science* **2017**, *356*, 599−604.

(21) Zhu, C.; Liu, T. Y.; Qian, F.; Han, T. Y. J.; Duoss, E. B.; Kuntz, J. D.; Spadaccini, C. M.; Worsley, M. A.; Li, Y. Supercapacitors Based on Three-Dimensional Hierarchical Graphene Aerogels with Periodic Macropores. *Nano Lett.* **2016**, *16*, 3448−3456.

DOI: 10.1021/acsomega.9b01833
ACS Omega 2019, 4, 15043−15050

(22) Xin, G. Q.; Yao, T. K.; Sun, H. T.; Scott, S. M.; Shao, D. L.; Wang, G. K.; Lian, J. Highly thermally conductive and mechanically strong graphene fibers. *Science* **2015**, *349*, 1083−1087.
(23) Wu, Q.; Chen, G. E.; Sun, W. G.; Xu, Z. L.; Kong, Y. F.; Zheng, X. P.; Xu, S. J. Bio-inspired GO-Ag/PVDF/F127 membrane with improved anti-fouling for natural organic matter (NOM) resistance. *Chem. Eng. J.* **2017**, *313*, 450−460.
(24) Lecaros, R. L. G.; Mendoza, G. E. J.; Hung, W. S.; An, Q. F.; Caparanga, A. R.; Tsai, H. A.; Hu, C. C.; Lee, K. R.; Lai, J. Y. Tunable interlayer spacing of composite graphene oxide-framework membrane for acetic acid dehydration. *Carbon* **2017**, *123*, 660−667.
(25) Huang, H. B.; Song, Z. G.; Wei, N.; Shi, L.; Mao, Y. Y.; Ying, Y. L.; Sun, L. W.; Xu, Z. P.; Peng, X. S. Ultrafast viscous water flow through nanostrand-channelled graphene oxide membranes. *Nat. Commun.* **2013**, *4*, No. 2979.
(26) Huang, K.; Liu, G. P.; Jin, W. Q. Vapor transport in graphene oxide laminates and their application in pervaporation. *Curr. Opin. Chem. Eng.* **2017**, *16*, 56−64.
(27) Liu, G. P.; Jin, W. Q.; Xu, N. P. Graphene-based membranes. *Chem. Soc. Rev.* **2015**, *44*, 5016−5030.
(28) Nair, R. R.; Wu, H. A.; Jayaram, P. N.; Grigorieva, I. V.; Geim, A. K. Unimpeded Permeation of Water Through Helium-Leak-Tight Graphene-Based Membranes. *Science* **2012**, *335*, 442−444.
(29) Li, W. B.; Wu, W. F.; Li, Z. J. Controlling Interlayer Spacing of Graphene Oxide Membranes by External Pressure Regulation. *ACS Nano* **2018**, *12*, 9309−9317.
(30) Han, L. F.; Xu, Z. L.; Cao, Y.; Wei, Y. M.; Xu, H. T. Preparation, characterization and permeation property of Al2O3, Al2O3-SiO2 and Al2O3-kaolin hollow fiber membranes. *J. Membr. Sci.* **2011**, *372*, 154−164.
(31) Xue, S. M.; Ji, C. H.; Xu, Z. L.; Tang, Y. J.; Li, R. H. Chlorine resistant TFN nanofiltration membrane incorporated with octadecylamine-grafted GO and fluorine-containing monomer. *J. Membr. Sci.* **2018**, *545*, 185−195.
(32) Cheng, X. X.; Pan, F. S.; Wang, M. R.; Li, W. D.; Song, Y. M.; Liu, G. H.; Yang, H.; Gao, B. X.; Wu, H.; Jiang, Z. Y. Hybrid membranes for pervaporation separations. *J. Membr. Sci.* **2017**, *541*, 329−346.
(33) Samei, M.; Iravaninia, M.; Mohammadi, T.; Asadi, A. A. Solution diffusion modeling of a composite PVA/fumed silica ceramic supported membrane. *Chem. Eng. Process.* **2016**, *109*, 11−19.
(34) Zhang, X.; Wang, M.; Ji, C. H.; Xu, X. R.; Ma, X. H.; Xu, Z. L. Multilayer Assembled CS-PSS/Ceramic Hollow Fiber Membranes for Pervaporation Dehydration. *Sep. Purif. Technol.* **2018**, *203*, 84−92.
(35) Ji, C. H.; Xue, S. M.; Xu, Z. L. Novel Swelling-Resistant Sodium Alginate Membrane Branching Modified by Glycogen for Highly Aqueous Ethanol Solution Pervaporation. *ACS Appl. Mater. Interfaces* **2016**, *8*, 27243−27253.
(36) Ma, X. H.; Zhang, H. X.; Gu, S. W.; Cao, Y.; Wen, X.; Xu, Z. L. Process optimization and modeling of membrane reactor using self-sufficient catalysis and separation of difunctional ceramic composite membrane to produce methyl laurate. *Sep. Purif. Technol.* **2014**, *132*, 370−377.
(37) Xie, H. R.; Ji, C. H.; Xue, S. M.; Xu, Z. L.; Yang, H.; Ma, X. H. Enhanced pervaporation performance of SA-PFSA/ceramic hybrid membranes for ethanol dehydration. *Sep. Purif. Technol.* **2018**, *206*, 218−225.
(38) Hung, W. S.; Chang, S. M.; Lecaros, R. L. G.; Ji, Y. L.; An, Q. F.; Hu, C. C.; Lee, K. R.; Lai, J. Y. Fabrication of hydrothermally reduced graphene oxide/chitosan composite membranes with a lamellar structure on methanol dehydration. *Carbon* **2017**, *117*, 112−119.
(39) Zhao, J.; Wang, F.; Pan, F. S.; Zhang, M. X.; Yang, X. Y.; Li, P.; Jiang, Z. Y.; Zhang, P.; Cao, X. Z.; Wang, B. Y. Enhanced pervaporation dehydration performance of ultrathin hybrid membrane by incorporating bioinspired multifunctional modifier and TiCl4 into chitosan. *J. Membr. Sci.* **2013**, *446*, 395−404.
(40) Yang, Q. Q.; Zhu, S. M.; Peng, W. H.; Yin, C.; Wang, W. L.; Gu, J. J.; Zhang, W.; Ma, J.; Deng, T.; Feng, C. L.; Zhang, D. Bioinspired Fabrication of Hierarchically Structured, pH-Tunable Photonic Crystals with Unique Transition. *ACS Nano* **2013**, *7*, 4911−4918.
(41) Ma, X. H.; Yao, Z. K.; Yang, Z.; Guo, H.; Xu, Z. L.; Tang, C. Y. Y.; Elimelech, M. Nanofoaming of Polyamide Desalination Membranes To Tune Permeability and Selectivity. *Environ. Sci. Technol. Lett.* **2018**, *5*, 123−130.
(42) Ma, X. H.; Yang, Z.; Yao, Z. K.; Guo, H.; Xu, Z. L.; Tang, C. Y. Y. Interfacial Polymerization with Electrosprayed Microdroplets: Toward Controllable and Ultrathin Polyamide Membranes. *Environ. Sci. Technol. Lett.* **2018**, *5*, 117−122.
(43) Kumar, S.; Koh, J. Synthesis, physiochemical and optical properties of chitosan based dye containing naphthalimide group. *Carbohydr. Polym.* **2013**, *94*, 221−228.
(44) Singh, J.; Dutta, P. K. Preparation, circular dichroism induced helical conformation and optical property of chitosan acid salt complexes for biomedical applications. *Int. J. Biol. Macromol.* **2009**, *45*, 384−392.
(45) Shi, Q.; Ni, L.; Zhang, Y.; Feng, X.; Chang, Q.; Meng, J. Poly(p-phenylene terephthamide) embedded in a polysulfone as the substrate for improving compaction resistance and adhesion of a thin film composite polyamide membrane. *J. Mater. Chem. A* **2017**, *5*, 13610−13624.
(46) Kong, X.; Qiu, Z.-L.; Lin, C.-E.; Song, Y.-Z.; Zhu, B.-K.; Zhu, L.-P.; Wei, X.-Z. High permselectivity hyperbranched polyester/polyamide ultrathin films with nanoscale heterogeneity. *J. Mater. Chem. A* **2017**, *5*, 7876−7884.
(47) Liu, Y. L.; Yu, C. H.; Lee, K. R.; Lai, J. Y. Chitosan/poly(tetrafluoroethylene) composite membranes using in pervaporation dehydration processes. *J. Membr. Sci.* **2007**, *287*, 230−236.
(48) Hung, W. S.; An, Q. F.; De Guzman, M.; Lin, H. Y.; Huang, S. H.; Liu, W. R.; Hu, C. C.; Lee, K. R.; Lai, J. Y. Pressure-assisted self-assembly technique for fabricating composite membranes consisting of highly ordered selective laminate layers of amphiphilic graphene oxide. *Carbon* **2014**, *68*, 670−677.
(49) Sajjan, A. M.; Kumar, B. K. J.; Kittur, A. A.; Kariduraganavar, M. Y. Novel approach for the development of pervaporation membranes using sodium alginate and chitosan-wrapped multiwalled carbon nanotubes for the dehydration of isopropanol. *J. Membr. Sci.* **2013**, *425*−*426*, 77−88.
(50) Premakshi, H. G.; Sajjan, A. M.; Kariduraganavar, M. Y. Development of pervaporation membranes using chitosan and titanium glycine-N,N-dimethylphosphonate for dehydration of isopropanol. *J. Mater. Chem. A* **2015**, *3*, 3952−3961.
(51) Zhao, Q.; Qian, J. W.; Zhu, C. X.; An, Q. F.; Xu, T. Q.; Zheng, Q.; Song, Y. H. A novel method for fabricating polyelectrolyte complex/inorganic nanohybrid membranes with high isopropanol dehydration performance. *J. Membr. Sci.* **2009**, *345*, 233−241.
(52) Zuo, J.; Shi, G. M.; Wei, S.; Chung, T. S. The Development of Novel Nexar Block Copolymer/Ultem Composite Membranes for C2-C4 Alcohols Dehydration via Pervaporation. *ACS Appl. Mater. Interfaces* **2014**, *6*, 13874−13883.

DOI: 10.1021/acsomega.9b01833
ACS Omega 2019, 4, 15043−15050